ACS OMEGA

http://pubs.acs.org/journal/acsodf

Article

Modeling Approach to Determine Static Rivulet Height in Regular Polygonal Capillary Tubes

Mansureh Kialashaki, Javad Sayyad Amin,* Omid Mohammadzadeh, and Sohrab Zendehboudi*

Cite This: *ACS Omega* 2022, 7, 9310−9321

Read Online

ACCESS | Metrics & More | Article Recommendations

ABSTRACT: The rise of partially wetting liquids along the corners of noncircular capillary tubes is observed in many practical science and engineering applications such as wastewater treatment using membranes, remediation, oil recovery from petroleum reservoirs, and blood flow. In this paper, rivulet rise at the corners of polygonal capillary tubes is studied for partially wetting liquids with contact angles below the critical value. The presence of corners changes the distribution of a liquid in an incomplete wetting condition. In this study, geometrical models are proposed to better understand the capillary rise and flow behavior at the corners. A geometrical solution for the capillary rivulet height and profile is derived under gravity in triangular, square, and pentagonal capillary tubes. The effects of several factors including contact angle, number of polygon sides, and liquid properties on the capillary rivulet height are examined. It was found that the ratio of liquid surface tension to density directly affects the corner rise, while it has an inverse relationship with other factors. The maximum rivulet height of 91.6 mm is obtained in the triangular capillary tube with a side length of 1 mm and a contact angle of 30° for polydimethylsiloxane (PDMS-20)-air fluid pair. The minimum capillary rivulet height of 6.2 mm, on the other hand, is achieved in the pentagonal capillary tube, with a side length of 3 mm and a contact angle of 30°. To validate the developed analytical approach, comparisons are made between the model results, literature predictions, and experimental data. In addition, the geometrical model for a square capillary tube is compared with previous published studies, revealing a good agreement. This study provides quantitative results for the influence of capillary tube shape on the flow behavior of fluids in noncircular tubes that can be useful for control and optimization of transport phenomena in corresponding systems.

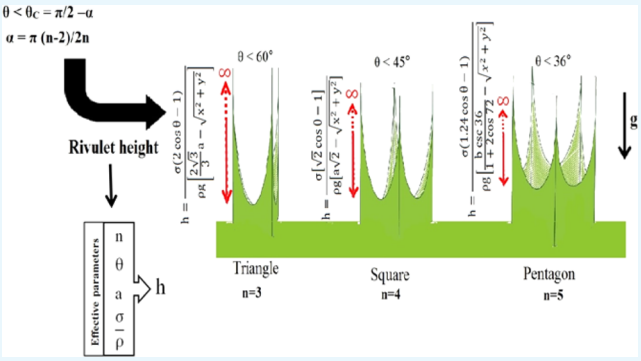

1. INTRODUCTION

Capillarity is a common and natural phenomenon that plays an important role in major engineering and science branches such as drying processes, remediation, capillary-driven heat pipes, capillary pumps, and crude oil extraction from reservoir rocks.[1,2] There are several studies in the literature on the experimental aspects of the capillary rise phenomenon. For instance, Siebold et al. (2000) experimentally investigated the effect of dynamic contact angle on the capillary rise phenomenon.[3] Extrand et al. (2013) measured the rising force of ethylene glycol, glycerol, and silica oil in glass and polytetrafluorethylene tubes with a tensiometer and correlated it with the capillary rise height.[4] Siebold et al. (1997) used capillary rise experimentation methods to thermodynamically characterize the irregular solid particle surfaces.[5] There are also several studies in the literature dealing with the theoretical aspects of the capillary rise phenomena. For instance, Wang et al. (2019) provided an analytical solution in the form of a dynamic model to predict the oscillatory behavior of the liquid rise in vertical capillaries.[1] A theory-based approach was also proposed by Liu et al. (2014) by which the maximum capillary rise in a porous sample was correlated with the contact angle, dry sample density and specific gravity, saturated sample hydraulic conductivity, and air entry height.[6] In another theoretical study, Gründing (2020) used mass and momentum balance to propose an enhanced model for the capillary rise problem.[2] In addition, some capillary rise experiments and numerical simulations were conducted by Khan et al. (2020) to investigate the spontaneous imbibition behavior of fluids in vuggy carbonates.[7]

The principle of capillary theory goes back to one century. Understanding the concept of capillary rise in porous media is very important because it is applicable in a wide variety of sciences and engineering disciplines.[8] Not all the practical

Received: November 2, 2021
Accepted: February 8, 2022
Published: March 14, 2022

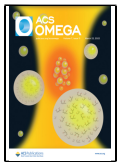

porous media prototypes are composed of capillaries with well-rounded spherical cross-sectional area. In practice, porous structures with capillaries of polygonal cross section are abundant in nature as well as in synthesized materials.[9] Therefore, it is essential to investigate fluid displacement under the effect of surface tension and gravity in polygonal capillary tubes since square and polygonal capillary tubes represent some of the smallest units of porous media.[10−12]

Analysis of liquid invasion through porous media corners has attracted much attention in various processes/cases such as oil recovery, pharmaceuticals, and biotechnology, especially with the application of microfluidic systems to study fluid flow and transport in porous structures. For instance, use of rectangular capillaries in microfluidic systems can increase heat and mass flux.[13−15] The cross-sectional geometry of a capillary influences the distribution of two immiscible liquid and gas phases.[16] In angular capillaries, for instance, the liquid (i.e., the wetting phase) invades the corner region, while the nonwetting gas phase remains at the center region, and a meniscus is created across the interface.[16,17]

Capillary behavior and meniscus rise in a cylindrical tube have been substantially studied experimentally and theoretically in numerous research works, and the proposed models are different from those of angular tubes.[15] For example, Lucas (1918) and Washburn (1921), for the first time, presented a solution for capillary rise in the absence of gravity effect, which better reveal the role of liquid properties such as surface tension in the liquid rise in capillary structures.[18−20] The Lucas−Washburn equations and Jurin's law (1728) are proposed for circular capillaries and should be modified for different pore geometries.[19−22] Rayleight and Bashfort-Adams calculated the static meniscus height and meniscus shape in the cylindrical geometry tube.[23,24]

The competition between the viscous and capillary forces affects the fluid penetration/flow in porous media. Capillary number is defined as the ratio of viscous forces to capillary forces. Capillary fingering, viscous fingering, and stable displacement are different types of fluid penetration in porous media. Depending on the viscosity of the invading as well as the displaced fluids, these three types of fluid penetration in porous media could occur.[25] Sarah and Ulrich (2018) measured liquid penetration in porous sheets using ultrasonic liquid penetration measurement, contact angle measurement, and scanning absorptiometry method.[26] 3D multiphase lattice Boltzmann model was also used by Shi et al. (2019) to investigate droplet and liquid penetration in porous structures.[27]

Analysis of capillary behavior in the complex geometry of porous media, with focus on corner structure problems, has been performed in various studies.[28] There are several experimental methods including mercury entrapment and gas sorption to directly map fluid distribution in a pore structure.[29] On the other hand, the models describing liquid rise in noncircular capillary geometries are more complicated and require intensive computations to include several factors such as nonuniform pore geometry as well as wetting properties.[28] Mayer (1965) and Stowe-Princen (1969) proposed the MS-P theory which determines the meniscus curvature in polygonal tubes with square and triangular cross-sections and a zero contact angle.[28,30] Mason and Morrow (1991) employed the MS-P method and carried out a survey on the curvature of the interface in irregular triangular tubes for complete wetting conditions.[31] They introduced a dimensionless shape factor (G) based on the perimeter and area of the cross-section and determined the equivalent shape factors for various geometries.[17,31] Ponomarenko et al. (2011) derived a general law for the capillary rise of wetting liquids in the corner of various geometries.[32]

Finding the correct meniscus curvature in different pore shapes is important because it changes the capillary pressure, and as a result, the displacement pattern in porous media will be affected.[33] The presence of corners in a porous structure affects the interface curvature; therefore, the capillary effect increases.[14] The curvature of interface menisci can be obtained by solving the well-known Yong−Laplace equation for capillary pressure.[34,35] The contact angle, the corner angle, and the relation between the vertical and horizontal characteristic lengths (i.e., which represent the magnitude of the capillary tube height and that of the tube radius, respectively) have a significant impact on the capillary pressure, and their role is demonstrated in transverse and axial curvature equations.[36] Long and Zhang (2017) analyzed the distribution of fluids and interface curvature based on single-corner capillary model in irregular capillary tubes.[31]

Concus and Finn (1974) introduced a method for determining the critical contact angle value (θ_c) in an n-sided regular polygon tube. This value depends on the polygonal corner angle. If the contact angle in partial wetting condition is below the critical value ($\theta < \theta_C = \pi/2 - \alpha$), where $\alpha = \pi\ (n-2)/2n$ is half of the corner angle, the meniscus rises along the corners to an infinite height, and rivulets or arc menisci appear in the corners. However, when the contact angle is equal to or greater than the critical angle value ($\theta \geq \theta_c$), the meniscus height is limited to a finite value, which refers to the bulk or pore meniscus, and rivulet rise does not appear along the corners.[30,37−43] The critical contact angle for the n-sided polygonal tube reaches zero, becoming similar to a circular tube shape as "n" approaches infinity, and the corner menisci will be vanished.[31] The rivulet rise in the corners and the increase in the corner menisci radius due to the increasing side number in regular capillary tubes are schematically shown in Figure 1.

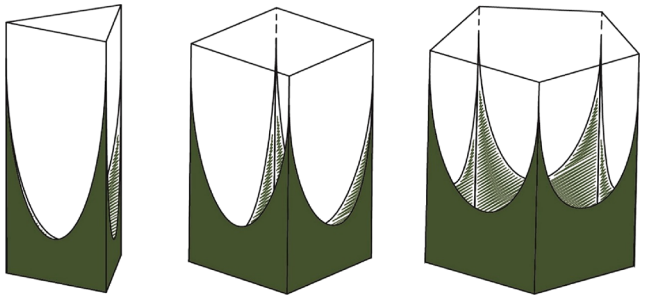

Figure 1. Schematic representation of rivulet rise and arc-menisci profiles in triangle, square, and pentagon capillary tubes.

Static capillary behavior at the corners of a capillary was also studied in the literature.[34,44−47] The 3D menisci shape, without considering gravity, was calculated in regular polygonal capillary tubes (i.e., with three, four, and six sides) as well as in rectangular capillary tubes from the augmented Young−Laplace equation by Wong et al. (1992). The researchers used a numerical method to eliminate the free boundary problem.[47] The iterative numerical method has been suggested instead of analytical methods in the literature to prevent solving a more

https://doi.org/10.1021/acsomega.1c06141
ACS Omega 2022, 7, 9310−9321

complex analytical integration.[21] Son et al. (2016) investigated the capillary rise in square and triangular tubes with a numerical lattice Boltzmann model.[30] Gurumurthy et al. (2018) simulated the spontaneous rise of a liquid phase in a square capillary using the InterFoam solver.[39] Hilden and Trumble (2003) numerically predicted the capillary pressure of liquids in planar close-packed spheres with the Surface Evolver software.[48]

Despite a few attempts on the analysis of the 3D interface shape in different cross-sectional geometries,[38] there is no general equation for determining the rivulet height in angular capillary tubes with consideration of the gravity effect. In this study, the geometrical method is applied using rivulet thickness for obtaining the rivulet height and shape of the menisci in triangle, square, and pentagon capillary tubes, considering the gravity effect. The developed models are then programmed in MATLAB R2014a, and the 3D menisci profiles are determined. In addition, the effects of various parameters such as the number of polygon sides, the contact angle, and the side length on the rivulet height are examined.

Liquid penetration in porous structures has attracted significant attention in various chemical processes. In this study, the quantitative results are used to investigate fluid displacement and the displacement pattern under the effect of surface tension and gravity in polygonal capillary tubes. The main goal of this study is to better understand the multiphase flow physics in porous media including capillaries with polygonal cross sections and offer a reliable and simple method that prevents solving a complex analytical integration problem.

The manuscript is structured as follows: in Section 2, the details of geometrical model development for triangular, square, and pentagonal capillary tubes are presented after a brief review of the literature. The shape of the menisci for various cross-sectional geometries is then determined by programming the developed geometrical model in MATLAB and is discussed in Section 3. A sensitivity analysis is then performed to study the impact of key parameters (such as the contact angle, the number of polygon sides, the capillary tube cross-sectional area, and the liquid properties) on the capillary rivulet height (Section 4). In Section 5, the developed geometrical models are validated by calculating the critical contact angle from the rivulet height equations, and the results are compared with the experimental data and values from the literature. Finally, the concluding remarks are presented in Section 6.

2. MODEL DEVELOPMENT

2.1. Rivulet Thickness Calculation—Literature Review. When a capillary tube is vertically dipped into a pool of liquid, the liquid phase moves upward in the tube in the z direction, against gravity, due to surface tension force, and therefore, a concave meniscus is developed whose radius of curvature depends on the degree of wetness of the capillary wall with the particular liquid phase. In such a condition, the rivulet is assumed to become static over a large time interval ($t \rightarrow \infty$), and the stationary solution can then be proposed to calculate the rivulet thickness. The rivulet thickness ($\delta(z)$), defined as the distance between the meniscus surface and the corner, was previously calculated for square tubes using a balance between the Laplace pressure and the hydrostatic pressure along the apparent contact line in the z direction.[39,49] The rivulet thickness varies along the height of the capillary tube from the bottom of the concave meniscus all the way to the maximum height of rivulet rise along the corners. The rivulet thickness in capillaries with triangle and pentagon cross-sections was also calculated based on the corner angle and the critical contact angle.[50] These correlations are reported in Table 1, where σ is the interfacial tension, θ is the contact angle between the meniscus and the wall, and ρ is the density difference between the liquid and air. These computations were confirmed with experimental measurements where the capillary tubes were dipped vertically in polydimethylsiloxane (PDMS-20) with a density of 930 kg/m^3 and a surface tension of 19.8 mN/m. The thickness equations are valid for $\theta < \theta_c$ where their values are positive. To simplify the calculations, the variation of curvature in the vertical direction was ignored, and only horizontal curvature related to the cross-sectional geometry was considered. It was also assumed that the liquid partially wets the capillary wall with a contact angle of $\theta < 90°$. In all these computations, the origin of the z coordinate (z_0) was located at the bottom of the concave meniscus, and the origins of the x and y coordinates were considered at the center of the polygon cross section.

Table 1. Rivulet Thickness, Half Corner Angle, and Critical Contact Angle for Regular Polygons

cross-section	half corner angle (α) (deg)	critical contact angle (θ_c) (deg)	rivulet thickness (δ)[39,50]
triangle	30	60	$\frac{\sigma(2\cos\theta - 1)}{\rho g(z + z_0)}$
square	45	45	$\frac{\sigma(\sqrt{2}\cos\theta - 1)}{\rho g(z + z_0)}$
pentagon	54	36	$\frac{\sigma(1.24\cos\theta - 1)}{\rho g(z + z_0)}$

2.2. Geometrical Method for Triangle, Square, and Pentagon Cross-Sectioned Capillary Tubes. To study the infinite rivulet rise in this paper, we consider three categories of polygonal cross sections: triangle, square, and pentagon. The shape and height of the rivulet, in the form of $z = f(x, y)$, for all (x,y) values in regular cross-sectional geometries are obtained in 3D Cartesian coordinates of x, y, and z. In order to derive a geometrical model for each capillary tube, a horizontal plane P is passed through the tubes' cross section. The intersecting area of the horizontal plane with the capillary tubes and the top view of the arc menisci are depicted in Figure 2. It should be noted that the rivulet height is not calculated at some distance from the corner; it is rather calculated at the corner. The rivulet thickness at the bulk meniscus height (i.e., δ) is indeed a function of the cross-section dimensions. The distance between each vertex of the polygon and the center of gravity (d) depends on the side length of the capillary (Figure 2a–c). This is based on simple trigonometric relations, as evident from Figure 2a–c. Therefore, a change in the side length will change the "d" parameter (see eqs 2, 7, and 10), which therefore changes the δ parameter. To develop and solve the equation for the rivulet height, the shape of the interface for all tubes is considered as circular at a certain elevation (i.e., z). The radius of the interface circle varies over the height as the thickness of the rivulet changes in the z direction due to the advancement of rivulet along the corners (Figure 3). The calculations below are conducted for only one corner of each

https://doi.org/10.1021/acsomega.1c06141
ACS Omega 2022, 7, 9310−9321

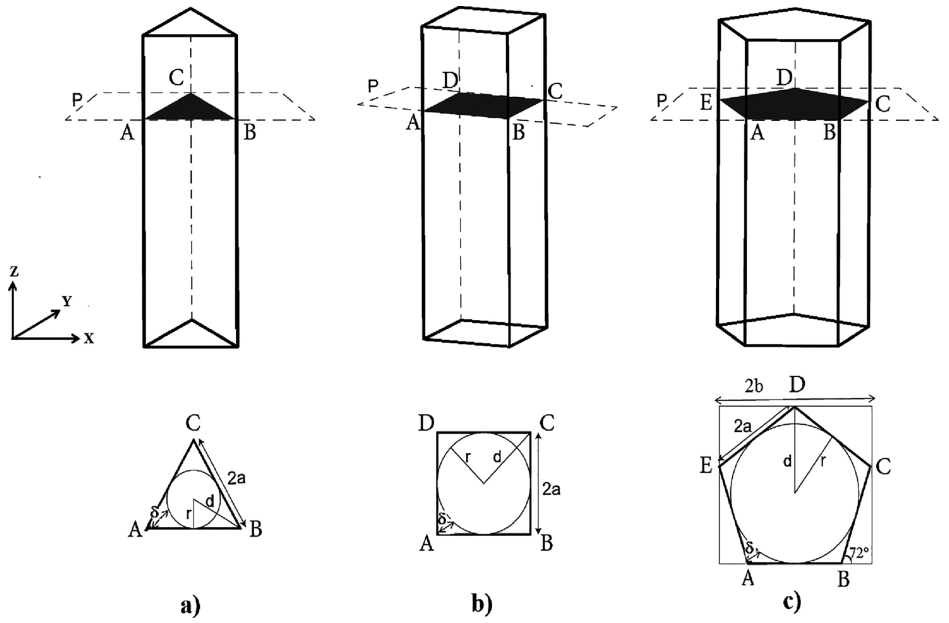

Figure 2. Cross-section geometry and top view of the arc menisci profile in (a) triangle, (b) square, and (c) pentagon capillary tubes.

cross section since all sides of the polygons have the same length.

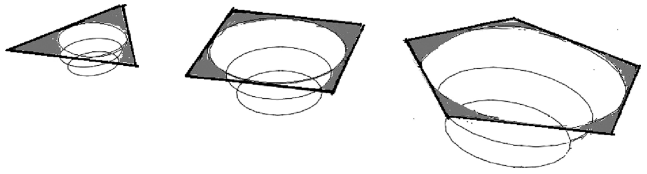

Figure 3. Development of the meniscus curvature in triangular, square, and pentagonal capillary tubes along the z-axis (top view).

2.2.1. Triangular Cross Section. In Figure 2a, the projection of the 3D interface in the horizontal $x-y$ plane forms the triangle ABC where each side's length is $2a$. In the triangle ABC, the origin of coordinates is placed at the center of gravity of the triangle. Using simple trigonometry, the coordinates of the three vertices are $A(-a,-\frac{\sqrt{3}}{3}a,z)$, $B(a,-\frac{\sqrt{3}}{3}a,z)$, and $C(0,\frac{2\sqrt{3}}{3}a,z)$. The coordinates for the center of gravity (G) can be determined considering positions of the three vertices of A, B, and C as follows

$$G\left(\frac{x_A + x_B + x_C}{3}, \frac{y_A + y_B + y_C}{3}, \frac{z_A + z_B + z_C}{3}\right) = (0,0,z) \quad (1)$$

The distance between each vertex and the center of gravity, d, is equal and can be calculated as follows

$$d = \sqrt{(x_G - x_A)^2 + (y_G - y_A)^2 + (z_G - z_A)^2} = \frac{2\sqrt{3}}{3}a \quad (2)$$

Simple trigonometric calculations involving Figure 2a result in the following equation

$$\frac{2\sqrt{3}}{3}a - \delta = r \quad (3)$$

where r is the radius of curvature of the meniscus. Plugging eq 3 into the rivulet thickness equation in the triangular tube from Table 1 leads to

$$z + z_0 = \frac{\sigma[2\cos\theta - 1]}{\rho g\left[\frac{2\sqrt{3}}{3}a - r\right]} \quad (4)$$

The radius of curvature of the meniscus is determined with a circle equation format (i.e., the inscribed circle in Figure 2) as follows

$$r = \sqrt{x^2 + y^2} \quad (5)$$

The distance between the rivulet tip and the bulk meniscus, which is rivulet height, can be obtained by plugging eq 5 into 4, as given below

$$z = \frac{\sigma(2\cos\theta - 1)}{\rho g\left[\frac{2\sqrt{3}}{3}a - \sqrt{x^2 + y^2}\right]} - z_0 \quad (6)$$

2.2.2. Square Cross Section. From the geometry of the square in Figure 2b, the following equation can be obtained in the $x-y$ coordinate

$$\sqrt{2a^2} - \delta = r \quad (7)$$

where a is the half-side length of the square capillary and r refers to the radius of horizontal curvature of the meniscus. The radius of curvature increases along the z direction as the thickness of the rivulet decreases by height, and its maximum is equal to the half of the square diameter where $\delta = 0$. By substituting the rivulet thickness in the square capillary from Table 1 in eq 7, the rivulet height is obtained as follows

$$z + z_0 = \frac{\sigma[\sqrt{2}\cos\theta - 1]}{\rho g[a\sqrt{2} - r]} \quad (8)$$

Using eq 5, eq 8 is converted to the following form

https://doi.org/10.1021/acsomega.1c06141
ACS Omega 2022, 7, 9310−9321

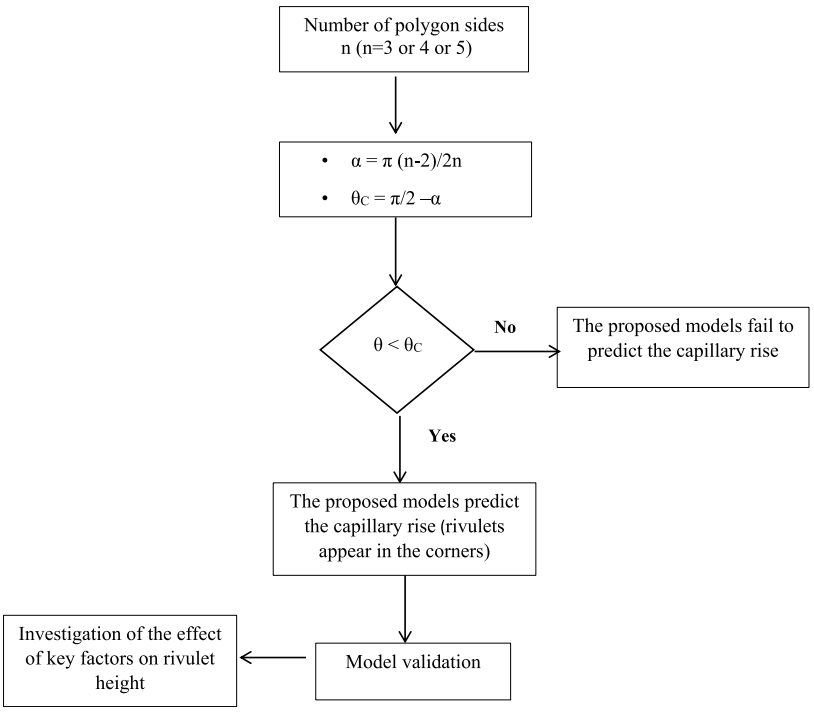

Figure 4. Main steps for obtaining the rivulet height in regular polygonal capillary tubes.

$$z = \frac{\sigma[\sqrt{2}\cos\theta - 1]}{\rho g[a\sqrt{2} - \sqrt{x^2 + y^2}]} - z_0 \quad (9)$$

2.2.3. Pentagonal Cross Section. The rivulet height in the pentagonal capillary tube (Figure 2c) can be determined similar to that for the triangle and square cross sections. The following equations are used where d is the radius of the circumscribed circle

$$d - \delta = r \quad (10)$$

$$a \csc 36 - \frac{\sigma(1.24\cos\theta - 1)}{\rho g(z + z_0)} = r \quad (11)$$

The pentagon cross section is inscribed in a square, where b is the half-length of the circumscribed square in Figure 2c. The relationship between the side length of the square and the pentagon tubes is given below

$$2a\ \cos 72 + a = b \quad (12)$$

$$a = \frac{b}{1 + 2\cos 72} \quad (13)$$

By substituting "a" (the half-length of the pentagon in Figure 2c) from eq 13 into eq 11 and also the rivulet thickness equation for the pentagon capillary tube (from Table 1), the rivulet height is obtained by the following expression

$$z + z_0 = \frac{\sigma(1.24\cos\theta - 1)}{\rho g\left[\frac{b\ \csc 36}{1 + 2\cos 72} - r\right]} \quad (14)$$

$$z = \frac{\sigma(1.24\cos\theta - 1)}{\rho g\left[\frac{b\ \csc 36}{1 + 2\cos 72} - \sqrt{x^2 + y^2}\right]} - z_0 \quad (15)$$

Figure 4 illustrates a simple algorithm for determination of the rivulet height in triangle, square, and pentagon cross-sectioned capillary tubes.

3. CALCULATIONS IN MATLAB

The models developed for calculation of the rivulet height in capillary tubes with various cross sections are programmed in MATLAB using surf (X, Y, Z) function. Matrices X and Y are defined based on the cross-section shape of the capillary tube, and a 0.01a-sized mesh (where a is the geometrical length based on Figure 2) is used in the X and Y directions to produce a grid. The liquid properties (density and surface tension), solid properties (height of the capillary tube), and liquid−solid properties (wetting contact angle) are included as initial input data in the MATLAB software to obtain the rivulet shape and height calculated based on the algorithms developed in this paper. The following assumptions/conditions are considered when developing these geometrical models:

1) For all three models developed in this study, the denominator would be undefined when the rivulet thickness reaches zero ($\delta = 0$). This implies that the thin liquid film does not exist at the corner. Under this assumption, the radius of curvature is equal to "d," giving an infinite height of the rivulet rise. However, it was proved by Mason and Morrow (1984) that the meniscus does not reach the corner of the regular polygon.[46] Wong et al. (1992) also considered a space filled with a thin liquid film between the wall and the meniscus (i.e., the precursor film assumption) to remove the contact line singularity.[47] Therefore, the assumption of zero rivulet thickness should be discarded. To rectify this issue in our models, it is assumed that the liquid films at the tip of the rivulet, around the corners of the polygon's cross-sections, are thin enough, and the 3D topology of the interfaces is plotted when the rivulet thickness (i.e., the intersecting point of liquid, gas, and solid) reaches a threshold value of 0.02a in all corners. The thickness of the liquid film between the walls and the meniscus is selected depending on the geometrical length. Since the

https://doi.org/10.1021/acsomega.1c06141
ACS Omega 2022, 7, 9310−9321

size of geometry does not lead to any error in our calculations, the same rational assumption is selected at different capillary lengths.
2) For all geometrical models, PDMS-20 is considered as the partially wetting liquid with a density of 930 kg/m^3 and a surface tension of 19.8 mN/m.
3) The gravity effect is considered in all models.
4) The proposed models fail to predict the capillary rise when the contact angle is equal to or greater than the critical contact angle associated with each geometry.
5) For all models, the Reynolds number is much smaller than unity; hence, the impact of inertial effects on rivulet flow can be ignored.

4. RESULTS AND DISCUSSION

From the geometrical model development section, it is clear that the rivulet height at the corners of the capillary tubes depends on several parameters such as the polygon cross-section shape (i.e., the number of polygon sides), the contact angle, and the side length (i.e., length of the base edge). According to the rivulet thickness equation in Table 1, $(2\cos\theta - 1)$, $(\sqrt{2}\cos\theta - 1)$, and $(1.24\cos\theta - 1)$ expressions appear in the numerator of the fraction for equations expressing rivulet rise in capillary tubes with triangle, square, and pentagon geometries, respectively. Thus, the rivulet thickness is positive for contact angle values smaller than the critical angle and becomes negative and/or undefined outside of this range. It also varies over the height of the capillary tube with an inverse proportionality as the height increases. This can be described as $\delta = K/z$, where K is the change in the rivulet thickness relative to the one at polygon cross section (i.e., height of the main meniscus). To calculate the radius of the inscribed circle in each polygon, matrices X and Y are defined based on the shape of the cross section for each capillary tube. It was found that the threshold mesh size is $0.03a$, where "a" is the half-side length of the capillary, through qualitative assessment of the 3D plots of the rivulet rise as well as the menisci profiles. The radius of the meniscus curvature is determined using a circle equation format ($r = \sqrt{x^2 + y^2}$). By selecting a fine mesh, the number of points in the matrices X and Y increases, which results in obtaining an accurate curve in the 3D profile. For mesh size values greater than $0.03a$, the 3D rivulet rise as well as menisci profiles are distorted with discontinuities in the perimeters. However, for the coarse mesh sizes equal to or smaller than $0.03a$, perfectly distinguishable profiles are obtained, with no sensitivity to mesh size in terms of the clarity of the profile perimeters. In other words, the mesh size affects the curvature and the 3D profiles of the menisci in all capillary tubes. The finer the mesh size, the larger the number of points in the matrices X and Y. This decreases the distance between the points, which leads to a higher resolution, that is, more accurate profiles. Therefore, a fine mesh size of $0.01a$ is selected in the x and y directions in order to generate mesh size-insensitive results. A schematic representation of the computational mesh size details along the x and y coordinates is demonstrated in Figure 5.

In the sections below, the impacts of various parameters on the rivulet profile and height are studied, and the minimum and maximum values of the corner rise are determined.

4.1. Effect of Polygon Shape. The cross-sectional geometry of the capillary tube has a great impact on the rivulet height. The 3D profiles of the menisci in the triangular, square, and pentagonal capillary tubes are shown in Figure 6. For the purpose of comparison, similar input values for the side length (i.e., 3 mm), wetting contact angle (30°), and fluid properties are used to compute menisci profiles in all capillary tubes. It is clear that the presence of corners affects the rivulet rise when the wetting contact angle (i.e., 30°) is less than the critical contact angle (i.e., 60, 45, and 36° for triangular, square, and pentagonal cross sections, respectively). The rivulet height is the same at all corners in each particular cross-sectional geometry. This is due to the fact that the capillary action increases in the corner region, which causes the rivulet to appear among the three phases.[43] It is also observed that the meniscus is concave for all three cross-sectional geometries. In addition, the menisci boundaries do not touch the corners of the cross sections (i.e., there are films of the wetting liquid occupying the corner spaces when the horizontal projections of the menisci are concerned in the x–y plane passing through at the bottom of the concave menisci), which satisfies assumption 1.

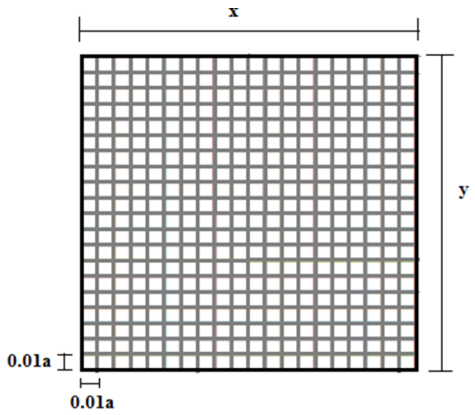

Figure 5. Schematic representation of the computational mesh size sensitivity aspect in the x and y directions.

For all capillary tubes, the arc meniscus advances in all corners, and the same behavior of the liquid film along the corner is observed in the models. Figure 6 clearly shows that the surface shape is a function of $z = f(x, y)$. Numerical solution of the proposed model gives the infinite rivulet heights (in z) in the corner (x, y) and finite rivulet height (in z) at the other (x, y) points in the cross section and on the perimeter.

From Figure 6, it is also observed that the radius of curvature for the meniscus increases along the z direction, while the liquid film thickness (i.e., rivulet thickness), close to the corner region, decreases by height. The thicker volume of the liquid film is situated near the bulk meniscus, and the liquid film at each corner becomes thinner at the tip position of the rivulet. Far from the bulk meniscus, the rivulet thickness is relatively insignificant. These observations are in agreement with the numerical simulation results presented by Gurumurthy et al. (2018).[39]

The rivulet height at the corners varies by changing the geometry of the capillaries' cross sections. The rivulet height lowers from 37.8 mm in the triangular capillary to 11.5 and 6.2 mm in the square and pentagon capillaries, respectively. It is concluded that the rivulet height at the corners has an inverse relation with the number of sides in regular polygonal capillary tubes. Since the contact angle for all three studied cases is less than the critical contact angle associated with each tube, rivulets appear at and rise along the corners.

https://doi.org/10.1021/acsomega.1c06141
ACS Omega 2022, 7, 9310−9321

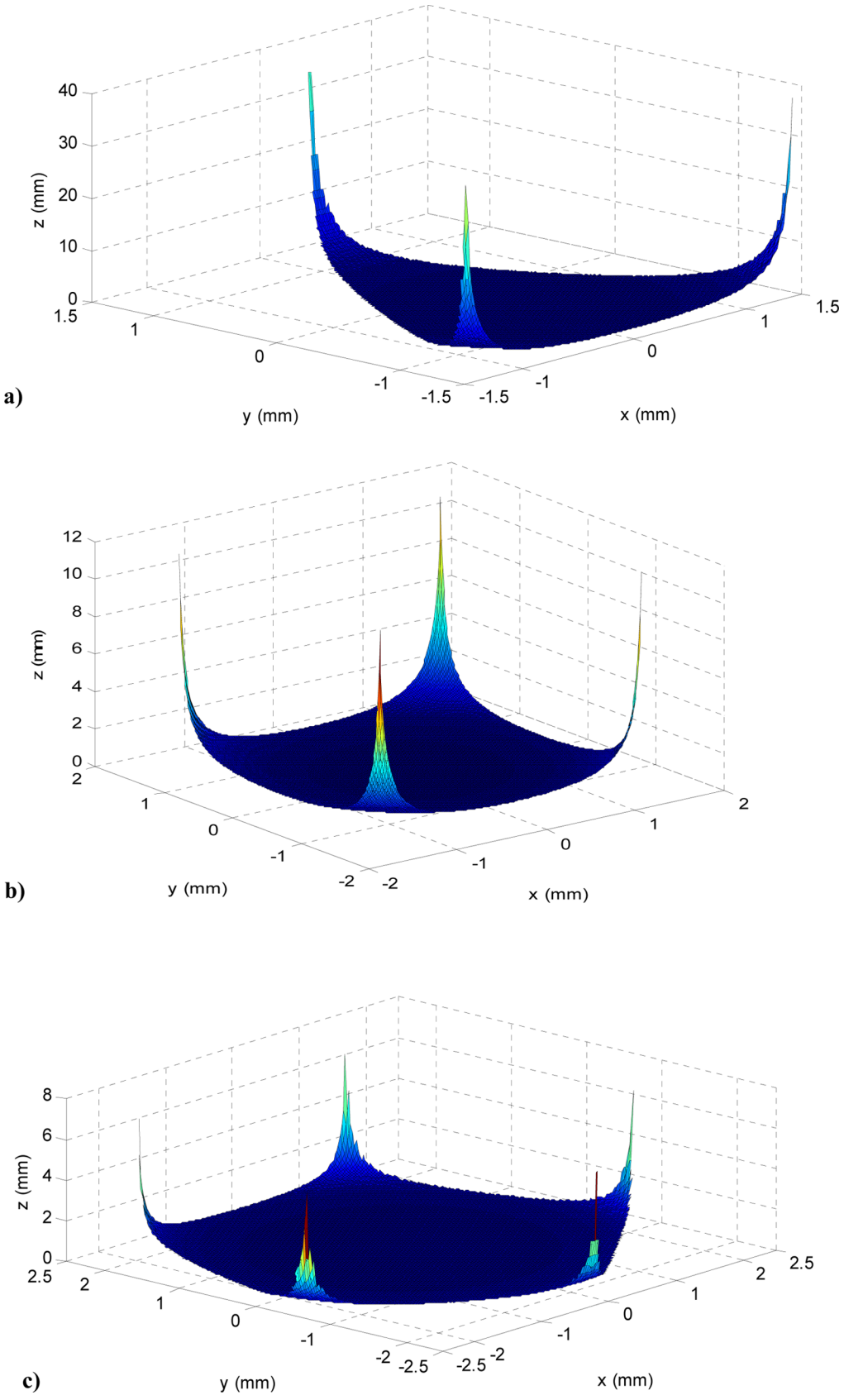

Figure 6. 3D plots of rivulet rise and menisci profiles in (a) triangle, (b) square, and (c) pentagon capillary tubes with a = 1.5 mm and θ = 30°.

4.2. Effect of Contact Angle. In order to understand the impact of contact angle on the rivulet height, three contact angle values of 0, 15, and 30° are examined when all other solid and liquid properties as well as the side length of the capillary cross section (i.e., 3 mm) are the same. Note that all these contact angle values are smaller than the critical contact angle

https://doi.org/10.1021/acsomega.1c06141
ACS Omega 2022, 7, 9310−9321

associated with each capillary tube. Figure 7 compares the rivulet profile and equilibrium height in one corner at different

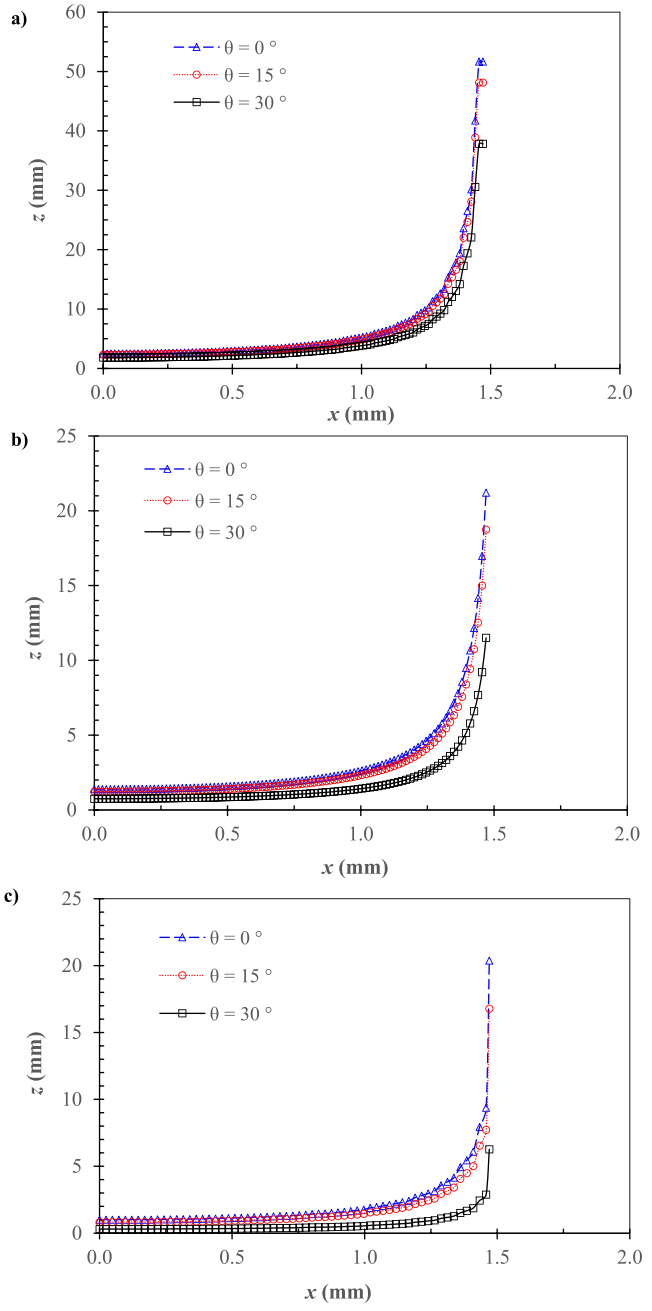

Figure 7. Effect of contact angle on the rivulet height for (a) triangle, (b) square, and (c) pentagon capillary tubes with a side length of 3 mm.

contact angles for various capillaries. It is clear that the contact angle has a significant impact on the meniscus profile in the $x-z$ plane (when the y coordinate is fixed, i.e., at a particular corner) as well as on the equilibrium rivulet height at the corner. The greater the contact angle value (i.e., the closer it gets to the critical contact angle for each particular cross-section geometry), the smaller the rivulet height at the corner. For circumstances where the solid surface is wetted better with the liquid (i.e., lower contact angle), the capillary action is greater in magnitude which results in greater spontaneous advancement of the liquid film edge at the corner and hence a higher rivulet height. The gas−liquid profiles displayed in Figure 6 also confirm assumption 1 according to which there is a liquid film occupying the corner; thus, the menisci circumference does not touch the solid surface. Rise of the height of liquid in the triangle capillary tube is obtained as 51.6, 48.1, and 37.8 mm at 0, 15, and 30°, respectively. In square and pentagon capillary tubes, more decline is observed. The height decreases to 21.2 and 20.3 mm at the contact angle of 0° for the square and pentagon capillaries, respectively. It continues to decrease to 18.7 and 16.7 mm at a contact angle of 15° and 11.5 and 6.2 mm at a contact angle of 30°. The lowest height of 6.2 mm is observed in the pentagon capillary tube at a contact angle of 30°.

The calculated rivulet height values are also plotted versus contact angle (Figure 8). A quadratic function is fitted to the

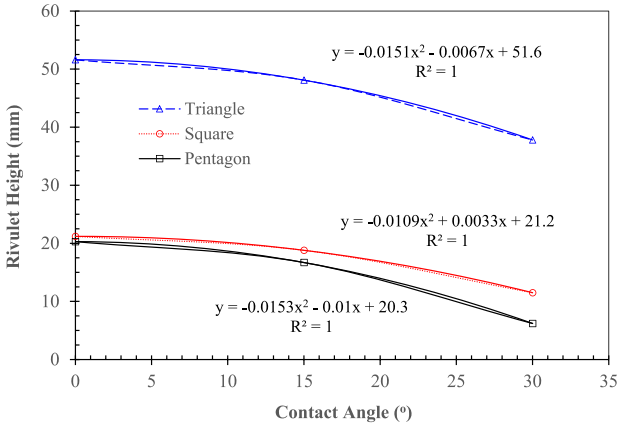

Figure 8. Change in rivulet height with contact angle for different capillary tubes.

calculated rivulet height values for each dataset associated with a particular capillary tube, with perfect correlation coefficients. The decreasing trend of the rivulet height versus contact angle is evident from the descending trends in Figure 8. The accuracy of our calculated rivulet height values can also be double checked by predicting the critical contact angle value for each capillary tube (where the rivulet height becomes negligible) from the trend-lines fitted on the datasets. One could approach the rivulet height to zero and solve the quadratic equation for each capillary tube, which results in critical contact angle values very close to those reported in Table 1.

4.3. Effect of Side Length. The side length of the capillary tube is found to significantly affect the height of rivulet rise at the corners. Three side lengths of 1, 2, and 3 mm are used in three capillary geometries at a fixed contact angle of 30°. The heights of rivulet rise at one particular corner (i.e., fixed y-coordinate) for the three capillary types are displayed in Figure 9. Clearly, the capillary rivulet rise at the corner has an inverse relation with the side length of the capillary. The greatest rivulet rise values are obtained in capillaries with less number of corners as well as the smallest side length. This is due to the fact that the smaller the side length of the capillary, the smaller the radius of curvature associated with the concave meniscus formed at the gas−liquid contact surface. This will lead to an increase in the capillary action which subsequently increases the height of capillary rise associated with the advancing rivulet

https://doi.org/10.1021/acsomega.1c06141
ACS Omega 2022, 7, 9310−9321

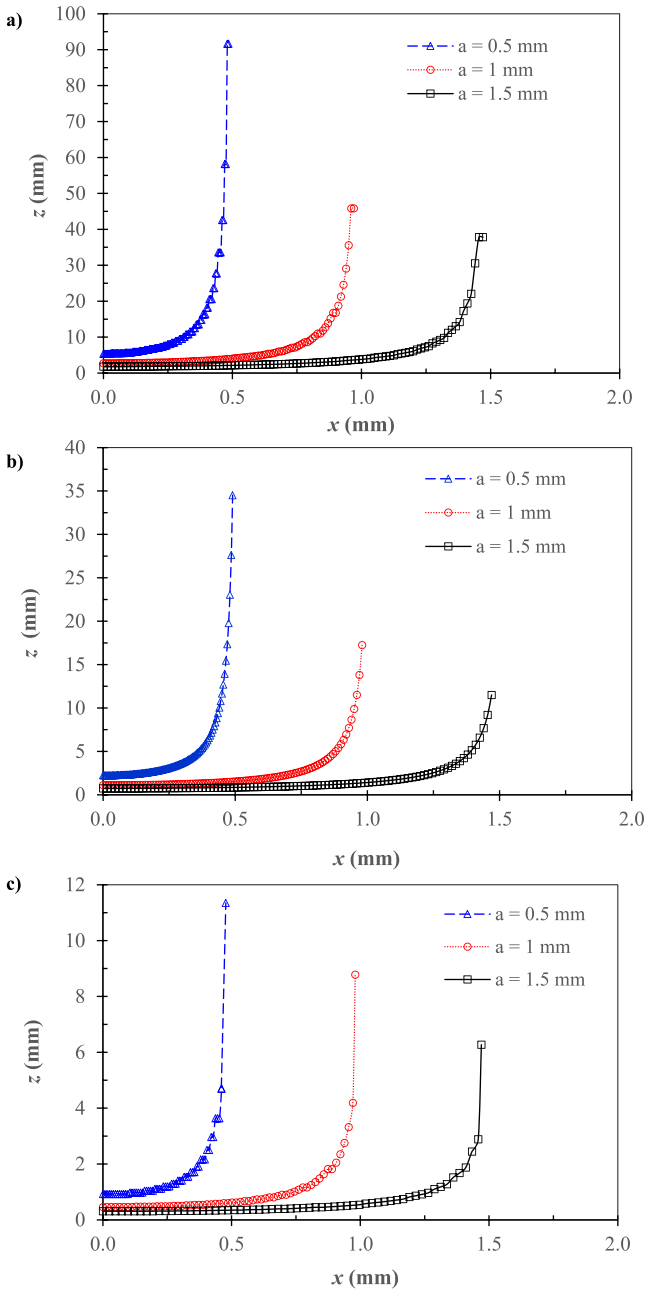

Figure 9. Effects of side length on the rivulet height at a contact angle of 30° for (a) triangle, (b) square, and (c) pentagon cross-section capillary tubes.

at the corners. This finding is in agreement with previous studies presented in the literature.[39]

4.4. Effect of Liquid Type. To investigate the impact of liquid properties (i.e., surface tension and density) on rivulet height calculations, we consider three types of liquids, namely, water, polydimethylsiloxane (a silicone oil) with kinematic viscosity of 20 and 100 cSt (PDMS-20 and PDMS-100), respectively, with the properties listed in Table 2. The effect of liquid properties on the rivulet capillary rise is summarized in Table 3. According to Tables 2 and 3, the greater the ratio of surface tension to density, the larger is the rivulet rise value. The smallest rivulet height values are obtained for the pentagon capillary tube dipped into PDMS-100. In all three proposed geometrical models, the rivulet height is governed by

Table 2. Properties of the Liquids Used in Rivulet Height Calculations

properties	PDMS-20	PDMS-100	water
surface tension (mN/m)	19.8	20.1	72
density (kg/m^3)	930	970	1000
surface tension to density ratio (m^3/s^2)	0.0213	0.0207	0.072

Table 3. Effect of Liquid Type on Rivulet Capillary Rise (Base Edge Length: 3 mm; Contact Angle: 0°)

	rivulet height (mm)		
liquid type	triangular	square	pentagon
PDMS-20	51.6	21.2	20.3
PDMS-100	50.1	20.6	19.7
water	174.4	71.7	68.6

the surface tension and density of the liquid. The impact of this ratio was also observed in stationary solution of the corner rise in the literature, and a similar conclusion was made.[39,51]

5. MODEL VALIDATION

To investigate the accuracy of the three geometrical models developed in this study, one may look at the predicted critical contact angles, obtained from curve fitting presented in Figure 8, and compare them with the literature values (Table 1). The positive root of the three quadratic equations from Figure 8 represents the critical contact angle at which the rivulet height becomes negligible. These values are obtained as 58.24, 44.25, and 36.09° for the triangle, square, and pentagon capillaries, respectively. The relative error between the calculated and literature values of these critical contact angles are 2.93, 1.67, and 0.25% for triangle, square, and pentagon capillary tubes, respectively. The very small relative error values, with respect to the literature data, suggest that the accuracy of our predictions is significant.

In addition, the experimental capillary heights measured in the triangular and square tubes are 172 and 70 mm for the water/air system, respectively, which are very close to the corresponding calculated values (174.4 and 71.7 mm as reported in Table 3). The average error percentage is about 2%, revealing a very good match between the predictions and experimental data.

Another way of validating our geometrical formulations is through a comparison with a recently published paper by Gerlach et al. (2020) that describes a stationary solution for the rivulet rise in a rounded corner square capillary tube.[51] The stationary solution proposed by Gerlach et al. (2020) is as follows

$$z_{max} = \frac{\sigma}{\rho g R_w} \frac{\sqrt{2\left(1 - \frac{\tan^2(\theta)}{(\tan^2(\theta)+1)}\right)} - 1}{(\sqrt{2} - 1)} \quad (16)$$

$$R_w = \frac{\delta}{\sqrt{2}\cos\theta - 1} \quad (17)$$

where R_w is the radius of curvature of the wetting liquid on the wall at the corner region.

Similar to our geometrical models (eqs 6, 9, and 15), the spontaneous capillary rise at the corners expressed by eq 16 is also governed by surface tension, gravity forces, and density.

https://doi.org/10.1021/acsomega.1c06141
ACS Omega 2022, 7, 9310−9321

The maximum rivulet rise height (z_{max}) is obtained from the stationary solution when $\theta = 0$, as shown below[51]

$$z_{max} = \frac{\sigma}{\rho g R_w} = \frac{\sigma}{\rho g}\left[\frac{(\sqrt{2}-1)}{\delta}\right] \quad (18)$$

Our geometrical model for rivulet height in a square capillary tube also suggests that the maximum capillary rise will occur at zero contact angle, as follows

$$z_{max} = \frac{\sigma(\sqrt{2}-1)}{\rho g(a\sqrt{2} - \sqrt{x^2+y^2})} - z_0 \quad (19)$$

It should be noted that the origin of the z coordinate (i.e., z_0) is located at the lowest point of the concave meniscus.

Comparison of the maximum rivulet rise height expressions from our geometrical model, eq 19, with that obtained from the stationary solution,[51] eq 18, suggests that the thickness of the rivulet in the stationary solution for the square capillary can be approximated by

$$\delta_{square-capillary} = a\sqrt{2} - \sqrt{x^2+y^2} \quad (20)$$

A review of Figure 2b clearly shows that the difference between the half diameter of square ($a\sqrt{2}$) and the radius of the inscribed circle ($r = \sqrt{x^2+y^2}$) is equal to the rivulet thickness. In other words, the relationship between the parameters included in our geometrical model, eq 9, is similar to the one proposed by Gerlach et al. (2020) in eq 16.

It should be emphasized that all methods presented in the literature to plot the rivulet rise in nonsquare capillaries have some deficiencies, and the absence of meniscus on the flat wall portions is the limitation of our model as mentioned in Figure 6. This error is resulted from the simplifying assumptions considered in this study. It is known that the curvature of the rivulet is also present in the vertical direction near the bulk meniscus; therefore, it would be better in general to consider this curvature in the vertical plane as well in order to obtain a more accurate rivulet rise. However at a large distance from the bulk meniscus, the rivulet thickness is insignificant; it is much smaller than the radius of meniscus. To simplify the final equations (eqs 6, 9, and 15), the horizontal curvature is only considered, based on which the remote stationary shape of the rivulet is obtained. The rivulet shape is estimated from the proposed rivulet thickness along the vertical centerline of the rivulet. It is not possible to calculate the vertical curvature using analytical methods. For the remote solution of the model, however, consideration of the horizontal curvature could provide an approximate rivulet height. This assumption was also used by Gurumurthy et al. (2018) by which the remote rivulet shape was obtained based on rivulet thickness using numerical methods.[39,43]

The capillary rise at the corners of capillary tubes has been the subject of numerous experimental, analytical, and simulation studies in the literature. Various scientific and engineering applications of noncircular capillary tubes make it inevitable to find a robust yet practical methodology to predict the rivulet rise and thickness in polygonal capillaries. The experimental methodologies are time consuming, could be challenging to execute for more complex geometries, and are subject to measurement errors. Use of mathematical modeling and geometrical relations, however, can provide an exact method to compute the rivulet rise and thickness, and determine the exact topology of the 3D menisci. The presented geometrical models could form the basis of a detailed yet quick methodology for computation of liquid rise in complex capillary corners.

6. CONCLUSIONS

The results of rivulet profile and tip position in the triangle, square, and pentagon capillary tubes under the effect of gravity are presented in this study. With the geometrical consideration of capillary tubes, the rivulet rise equations for a partially wetting condition are developed, and the algorithms are introduced in MATLAB software to plot the 3D surfaces of menisci. The following conclusions are obtained from this study

- Based on our analytical solution, the corner meniscus rises when the contact angle is below its critical value. In all three capillary tube geometries, the rivulet advances close to the intersecting point of the liquid, gas, and solid. The radius of curvature for the meniscus increases, and the rivulet thickness decreases along the z direction.
- It is observed that the menisci are all concave, and the rivulet height is the same at all corners for each particular capillary tube.
- It is found that the number of polygon sides, the contact angle, and the side length inversely affect the corner rise. Upon an increase in the contact angle, a quadratic function is able to closely predict the rivulet height for each particular capillary tube.
- Investigating the impact of liquid type on the height of rivulet rise reveals that the height is directly related to the ratio of surface tension to density of the liquid.
- In order to validate the geometrical models, the critical contact angle values are calculated by solving the quadratic equations describing the change of rivulet height versus contact angle. The calculated values of the critical contact angle are in agreement with the values reported in the literature. A comparison between the experimental and predicted rivulet height in triangular and square tubes also show very good agreement. In addition, the model of rivulet capillary rise in the square capillary tube is compared against another formulation presented in the literature, and both methodologies result in a similar relationship between the model parameters and almost the same results.
- For more complicated capillary tube geometries, the exact analysis of the rivulet profile is a relatively difficult task. For such cases, it is recommended to numerically simulate the 3D rivulet shape and profile in order to better visualize the corner rise as well as the 3D topology of the interface. The analytical model proposed in this study could also be generalized for the case of "n" corners.

7. EXPERIMENTAL PHASE

A simple experimental setup is designed to measure rivulet capillary rise in two noncircular capillary tubes, namely, triangular and square (see Figure 10). The pentagonal capillary was not available in our lab to conduct tests. The capillary rise measurements in only two capillary tubes are adequate for comparison and validation purposes.

A proper stand/holder was designed to firmly hold the capillary tubes in the vertical direction. To attain zero contact

https://doi.org/10.1021/acsomega.1c06141
ACS Omega 2022, 7, 9310−9321

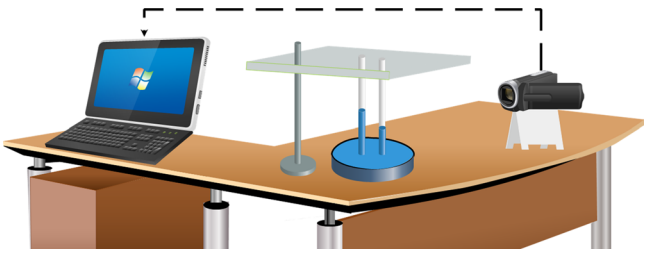

Figure 10. Simple schematic of the experimental setup used in this research.

angle, deionized water was used in the experiments, and the internal surface of the glass tubes was carefully cleaned before each experimental run. This was confirmed in the tests as the measured contact angles were all lower than 10°. The capillary tubes were dipped in a water container so that water can easily enter the tubes. A high-speed camera (Panasonic Lumix DMC-FZ300 Digital Camera) was used to record the liquid-rising process in the tubes. The capillary rise was measured from the point that the tube touched water to the point where the meniscus stopped. An image processing software helped to find the instantaneous and equilibrium capillary heights over the process. The equilibrium capillary height can also be measured using a ruler in a simple way. Each test was repeated three times, and the average heights are calculated and reported in this work. The possible errors in the experiments were measurement errors and the presence of contaminants in the tubes and water.

AUTHOR INFORMATION

Corresponding Authors

Javad Sayyad Amin − *Department of Chemical Engineering, University of Guilan, Rasht 41996-13769, Iran*; Email: sayyadamin@guilan.ac.ir, sayyadamin@gmail.com

Sohrab Zendehboudi − *Faculty of Engineering and Applied Science, Memorial University, St. John's, Newfoundland and Labrador A1C 5S7, Canada*; orcid.org/0000-0001-8527-9087; Email: szendehboudi@mun.ca

Authors

Mansureh Kialashaki − *Department of Chemical Engineering, University of Guilan, Rasht 41996-13769, Iran*

Omid Mohammadzadeh − *Faculty of Engineering and Applied Science, Memorial University, St. John's, Newfoundland and Labrador A1C 5S7, Canada*

Complete contact information is available at: https://pubs.acs.org/10.1021/acsomega.1c06141

Notes

The authors declare no competing financial interest.

ACKNOWLEDGMENTS

The authors wish to thank the University of Guilan for supporting the graduate student involved in the project.

ABBREVIATIONS

Letters/variables

a, half-length of polygon, m
A, B, C, D and E, vertex coordinates, m
b, half-length of the circumscribed square, m
d, distance between each vertex and the center of gravity, m
g, gravitational acceleration, m/s^2
G, center of gravity, dimensionless
K, constant, dimensionless
n, number of polygon sides, dimensionless
r and R_w, curvature radius of meniscus, m
z, rivulet height, m
z_0, origin of the z coordinate (i.e., the bottom of the concave meniscus), m
Z_{max}, maximum rivulet rise height, m

Greek symbols

θ_c, critical contact angle, degrees
α, half corner angle, degrees
σ, surface tension, mN/m
θ, contact angle between the meniscus and the wall, degrees
ρ, density, kg/m^3
δ, rivulet thickness, m

REFERENCES

(1) Wang, Q.; Li, L.; Gu, J.; Weng, N. A dynamic model for the oscillatory regime of liquid rise in capillaries. *J. Chem. Eng. Sci.* **2019**, *209*, 115220.

(2) Gründing, D. An enhanced model for the capillary rise problem. *Int. J. Multiph. Flow.* **2020**, *128*, 103210.

(3) Siebold, A.; Nardin, M.; Schultz, J.; Walliser, A.; Oppliger, M. Effect of dynamic contact angle on capillary rise phenomena. *Colloids Surf., A* **2000**, *161*, 81−87.

(4) Extrand, C. W.; Moon, S. I. Experimental measurement of forces and energies associated with capillary rise in a vertical tube. *J. Colloid Interface Sci.* **2013**, *407*, 488−492.

(5) Siebold, A.; Walliser, A.; Nardin, M.; Oppliger, M.; Schultz, J. Capillary rise for thermodynamic characterization of solid particle surface. *J. Colloid Interface Sci.* **1997**, *186*, 60−70.

(6) Liu, Q.; Yasufuku, N.; Miao, J.; Ren, J. An approach for quick estimation of maximum height of capillary rise. *Soils Found.* **2014**, *54*, 1241−1245.

(7) Khan, H. J.; Mehmani, A.; Prodanović, M.; DiCarlo, D.; Khan, D. J. Capillary rise in vuggy media. *Adv. Water Resour.* **2020**, *143*, 103671.

(8) Zhmud, B. V.; Tiberg, F.; Hallstensson, K. Dynamics of capillary rise. *J. Colloid Interface Sci.* **2000**, *228*, 263−269.

(9) Hamdan, M. O.; Abu-Nabah, B. A. Modeling meniscus rise in capillary tubes using fluid in rigid-body motion approach. *Commun. Nonlinear Sci. Numer. Simul.* **2018**, *57*, 449−460.

(10) Heshmati, M.; Piri, M. Experimental investigation of dynamic contact angle and capillary rise in tubes with circular and noncircular cross sections. *Langmuir* **2014**, *30*, 14151−14162.

(11) Latva-Kokko, M.; Rothman, D. H. Static contact angle in lattice Boltzmann models of immiscible fluids. *Phys. Rev. E.* **2005**, *72*, 046701.

(12) Schweigler, K. M.; Seifritz, S.; Selzer, M.; Nestler, B. Evaporation rate analysis of capillaries with polygonal cross-section. *Int. J. Heat Mass Transfer* **2018**, *121*, 943−951.

(13) Dong, M.; Chatzis, I. The imbibition and flow of a wetting liquid along the corners of a square capillary tube. *J. Colloid Interface Sci.* **1995**, *172*, 278−288.

(14) Higuera, F. J.; Medina, A.; Liñán, A. Capillary rise of a liquid between two vertical plates making a small angle. *Phys. Fluids.* **2008**, *20*, 102102.

(15) Wu, P.; Zhang, H.; Nikolov, A.; Wasan, D. Rise of the main meniscus in rectangular capillaries: Experiments and modeling. *J. Colloid Interface Sci.* **2016**, *461*, 195−202.

(16) Long, L.; Li, Y.; Dong, M. Liquid−Liquid Flow in Irregular Triangular Capillaries Under Different Wettabilities and Various Viscosity Ratios. *Transp. Porous Media* **2016**, *115*, 79−100.

(17) Sherwood, J. D.; Lac, E. Streaming potential generated by two-phase flow in a polygonal capillary. *J. Colloid Interface Sci.* **2010**, *349*, 417−423.

(18) Lucas, R. Rate of capillary ascension of liquids. *Kolloidn. Zh.* **1918**, *23*, 15−22.
(19) Washburn, E. W. The dynamics of capillary flow. *Phys. Rev.* **1921**, *17*, 273.
(20) Fries, N.; Dreyer, M. An analytic solution of capillary rise restrained by gravity. *J. Colloid Interface Sci.* **2008**, *320*, 259−263.
(21) Cai, J.; Perfect, E.; Cheng, C.-L.; Hu, X. Generalized modeling of spontaneous imbibition based on Hagen−Poiseuille flow in tortuous capillaries with variably shaped apertures. *Langmuir* **2014**, *30*, 5142−5151.
(22) Barozzi, G. S.; Angeli, D. A note on capillary rise in tubes. *Energy Procedia* **2014**, *45*, 548−557.
(23) Rayleigh, L. On the theory of the capillary tube. *Proc. R. Soc. London.* **1916**, *92*, 184−195.
(24) Jiang, J.; Guo, Q.; Wang, B.; Zhou, L.; Xu, C.; Deng, C.; Yao, X.; Su, Y.; Wang, J. Research on variation of static contact angle in incomplete wetting system and modeling method. *Colloids Surf., A* **2016**, *504*, 400−406.
(25) Perazzo, A.; Tomaiuolo, G.; Preziosi, V.; Guido, S. Emulsions in porous media: From single droplet behavior to applications for oil recovery. *Adv. Colloid Interface Sci.* **2018**, *256*, 305−325.
(26) Sarah, K.; Ulrich, H. Short timescale wetting and penetration on porous sheets measured with ultrasound, direct absorption and contact angle. *RSC Adv.* **2018**, *8*, 12861−12869.
(27) Shi, Y.; Tang, G. H.; Lin, H. F.; Zhao, P. X.; Cheng, L. H. Dynamics of droplet and liquid layer penetration in three-dimensional porous media: A lattice Boltzmann study. *Phys. Fluids* **2019**, *31*, 042106.
(28) Ma, S.; Mason, G.; Morrow, N. R. Effect of contact angle on drainage and imbibition in regular polygonal tubes. *Colloids Surf., A* **1996**, *117*, 273−291.
(29) Tsakiroglou, C. D.; Burganos, V. N.; Jacobsen, J. Pore-structure analysis by using nitrogen sorption and mercury intrusion data. *AIChE J.* **2004**, *50*, 489−510.
(30) Son, S.; Chen, L.; Kang, Q.; Derome, D.; Carmeliet, J. Contact angle effects on pore and corner arc menisci in polygonal capillary tubes studied with the pseudopotential multiphase Lattice Boltzmann model. *Computation* **2016**, *4*, 12.
(31) Long, L.; Zhang, B. The distribution of fluids in irregular capillary tubes: a new capillary model based on the single-corner capillary. *J. Pet. Explor. Prod. Technol.* **2018**, *8*, 341.
(32) Ponomarenko, A.; Quéré, D.; Clanet, C. A universal law for capillary rise in corners. *J. Fluid Mech.* **2011**, *666*, 146−154.
(33) Liu, Y.; Hansen, A.; Block, E.; Morrow, N. R.; Squier, J.; Oakey, J. Two-phase displacements in microchannels of triangular cross-section. *J. Colloid Interface Sci.* **2017**, *507*, 234−241.
(34) Mason, G.; Morrow, N. R. Capillary behavior of a perfectly wetting liquid in irregular triangular tubes. *J. Colloid Interface Sci.* **1991**, *141*, 262−274.
(35) Kim, P.; Kim, H.-Y.; Kim, J. K.; Reiter, G.; Suh, K. Y. Multi-curvature liquid meniscus in a nanochannel: Evidence of interplay between intermolecular and surface forces. *Lab Chip* **2009**, *9*, 3255−3260.
(36) Yang, L.; Homsy, G. M. Steady three-dimensional thermocapillary flows and dryout inside a V-shaped wedge. *Phys. Fluids* **2006**, *18*, 042107.
(37) Concus, P.; Finn, R. On capillary free surfaces in the absence of gravity. *Acta Math.* **1974**, *132*, 177−198.
(38) Feng, J.; Rothstein, J. P. Simulations of novel nanostructures formed by capillary effects in lithography. *J. Colloid Interface Sci.* **2011**, *354*, 386−395.
(39) Thammanna Gurumurthy, V.; Rettenmaier, D.; Roisman, I. V.; Tropea, C.; Garoff, S. Computations of spontaneous rise of a rivulet in a corner of a vertical square capillary. *Colloids Surf., A* **2018**, *544*, 118−126.
(40) Collicott, S. H.; Weislogel, M. M. Computing existence and stability of capillary surfaces using Surface Evolver. *AIAA J.* **2004**, *42*, 289−295.
(41) Li, J.; Chen, X.; Huang, Y.; Bai, Y. Study on asymmetric interior corner flow in microgravity condition. *Sci. China Technol. Sci.* **2012**, *55*, 2332−2337.
(42) Ajaev, V. S.; Homsy, G. M. Modeling shapes and dynamics of confined bubbles. *Annu. Rev. Fluid Mech.* **2006**, *38*, 277−307.
(43) Thammanna Gurumurthy, V.; Roisman, I. V.; Tropea, C.; Garoff, S. Spontaneous rise in open rectangular channels under gravity. *J. Colloid Interface Sci.* **2018**, *527*, 151−158.
(44) Langbein, D. The shape and stability of liquid menisci at solid edges. *J. Fluid Mech.* **1990**, *213*, 251−265.
(45) Concus, P.; Finn, R. On the behavior of a capillary surface in a wedge. *PNAS* **1969**, *63*, 292.
(46) Mason, G.; Morrow, N. R. Meniscus curvatures in capillaries of uniform cross-section. *J. Chem. Soc., Faraday Trans.* **1984**, *80*, 2375−2393.
(47) Wong, H.; Morris, S.; Radke, C. J. Three-dimensional menisci in polygonal capillaries. *J. Colloid Interface Sci.* **1992**, *148*, 317−336.
(48) Hilden, J. L.; Trumble, K. P. Numerical analysis of capillarity in packed spheres: Planar hexagonal-packed spheres. *J. Colloid Interface Sci.* **2003**, *267*, 463−474.
(49) Weislogel, M. M.; Lichter, S. Capillary flow in an interior corner. *J. Fluid Mech.* **1998**, *373*, 349−378.
(50) Tang, L.-H.; Tang, Y. Capillary rise in tubes with sharp grooves. *J. Phys. II* **1994**, *4*, 881−890.
(51) Gerlach, F.; Hussong, J.; Roisman, I. V.; Tropea, C. Capillary rivulet rise in real-world corners. *Colloids Surf., A* **2020**, *592*, 124530.

https://doi.org/10.1021/acsomega.1c06141
ACS Omega 2022, 7, 9310−9321